An Investigation of Additive Manufactured Silicon Carbide Ceramics for Body Armor Applications

Tyrone L. Jones[1], Jerry LaSalvia[1], Nicholas Ku[1], Kristopher Behler[1], Douglas Harris[1], Bill Goodman[2], Shawn Kelso[2], Mehrdad N. Ghasemi Nejhad[3], Brenden M. Minei[3]

[1]US Army Research Laboratory, Aberdeen Proving Ground, MD, 21005-5066, USA, tyrone.l.jones20.civ@mail.mil
[2]Goodman Technologies, Albuquerque, New Mexico 87109
[3]Hawai'i Nanotechnology Labs, Department of Mechanical Engineering, University of Hawai'i at Manoa, 2540 Dole St. Holmes Hall 302, Honolulu, Hawaii 96822

Abstract. The US Army and a Goodman Technologies Small Business and University team evaluated the mechanical properties and ballistic integrity of 3-D printed ceramic armor plates, fabricated using a novel additive manufacturing method. The method involved a proprietary z-process of nanopastes and subsequent ceramization in a vacuum furnace using 5 cycles of polymer infiltration pyrolysis (PIP) to compare the results with traditionally manufactured armor. The processed armor formulations concluded from a design of experiments (DOE) had a composition of: SiC-Si-B6O-BN-SiC-whiskers- SMP-10 nanopaste. Next, plates (90 mm × 90 mm × 8 mm) were manufactured, employing the z-process method, for ballistic analysis in accordance with established ballistic characterization procedures, using a 50.8 mm thick Aluminum 6061 plate as backing and witness plates in the case of penetration or deformation. Six alumina plates were examined ballistically (one shot per plate) against the 12.7 mm APM2 projectile (45.9 g) at an impact velocity of 840 m/s.

1. Introduction

1.1 Filling a Critical Need of the Army Advanced Manufacturing Initiative

October 4, 2019 the Secretary of the Army Ryan D. McCarthy has approved a new policy on advanced manufacturing that will help the Army secure a competitive edge against near-peer adversaries [1]. It is Army Directive 2019-29 "Enabling Readiness and Modernization through Advanced Manufacturing, also called the Army Advanced Manufacturing Initiative (AAMI) [2]. The AAMI is in accordance with the President's Executive Order 13329 (69 FR 9181) entitled "Encouraging Innovation in Manufacturing", the Related (Research and Research and Development) [3].

1.2 The AAMI policy has three key principles:

1. Strategic Investment: The Army must develop a holistic, threat-based strategy for the investment in and use of advanced methods and materials. Executing the strategy will require partnership from the private sector. As such, the policy allows for incentives designed to promote industry investment in advanced technologies.

2. Systemic Adoption: The Army will incorporate advanced manufacturing upfront and throughout a system's lifecycle.

3. Deliberate and Thoughtful Use: When using advanced manufacturing, be mindful of things like: intellectual property implications and return on investment.

1.3 Advanced manufacturing will promote the Army's ability to:

• Increase system performance through lighter and stronger materials.
• Decrease design limitations imposed by traditional methods -- design for performance, not manufacturability.

https://doi.org/10.52202/078352-0001

• Produce complex components as one piece, reducing failure points and increasing reliability.
• Reduce development time by rapidly producing prototypes and quickly transitioning them to production.
• Reduce risk of obsolete parts and diminishing sources of supply.
• Fabricate closer to the point-of-need, when needed.

The work conducted during the Phase I and II projects by the US Army Research Laboratory and Goodman Technologies (GT), has retroactively addressed the AAMI policy. The armor technology that was developed, GT RoboArmor™, fills an Army Critical Gap need by the additive manufacturing of lightweight silicon carbide ceramic matrix nanocomposites armor in form fitting shapes, and at the Point-of-Need. This is a capability that does not presently exist in industry. "Advanced manufacturing enhances the supply chain and sustainment efforts, both forward in the field and in our maintenance depots, enabling Soldiers to quickly manufacture critical parts and supplies at the point of need," said Gen. Gus Perna, commanding general of U.S. Army Materiel Command [1].

2. Experimental Methodologies

2.1 Material Methodologies

All characterization of the material was conducted on the manufactured plates employing the proprietary z-process method developed with Goodman Technologies and the University of Hawaii. Sample densities were determined using the Archimedes' principle. Sample composition was determined using a Bruker D8 Discover (Billerica, MA) X-ray diffractometer. The plate was also machined and polished to expose cross-sections that were perpendicular as well as parallel to the z-process axis. The microstructure of the plates was then determined by optical and scanning electron microscopy imaging of the cross-sections.

2.2 Dynamic Impact Failure Mechanism Model

Depth of Penetration (DOP) or residual penetration experiments were designed to determine the relative ballistic performance of different ceramic materials. For DOP testing, a projectile is fired into a ceramic tile attached to a thick metal backer plate such that the projectile will not deform the back surface of the metal plate. These experiments avoid the fundamental problem of V_{50} ballistic dependence on armor design (e.g. front-to-back plate ratio and material), require fewer shots than V50 tests, and have a sensitivity equivalent to that of other ballistic test methods. The change in penetration into the metal plates provides a comparison by which to rank the performance of the ceramic materials.

The target configuration used for these experiments is illustrated in Figure 1. The target consisted of a 90mm x 90mm ceramic tile at a thickness of 8mm, backed by two backup plates of aluminum alloy 6061 (AA6061, MIL-DTL-32262) plates of 50.8mm (2-inch) thickness. An epoxy resin, Dureflex® Optical Aliphatic Polyether Polyurethane Grade A4700, was used to attach each tile to the first (50.8mm) 2-inch plate. AA6061 was chosen as a well-characterized and readily available backer material. The aluminum backer plates were also expected to provide better resolution than steel plates. No cover plate was employed.

https://doi.org/10.52202/078352-0001

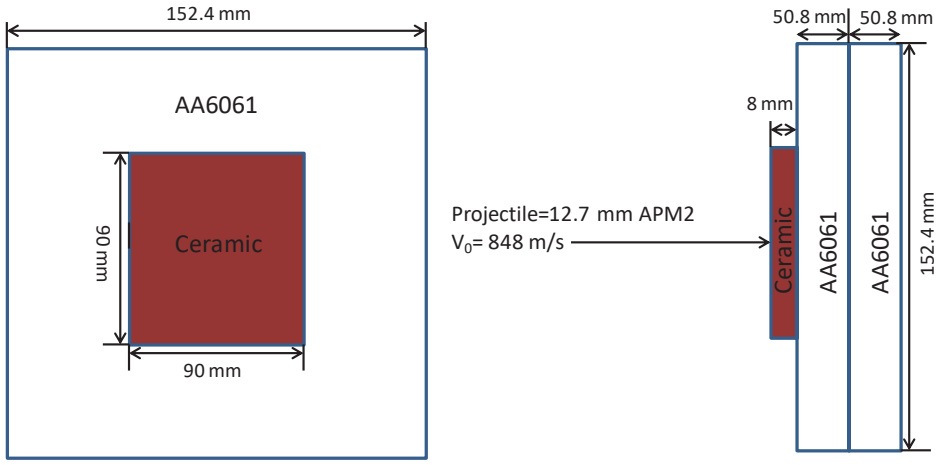

A) Front view B) Side View

Figure 1. Ceramic DOP target assembly.

All ballistic impact experiments were conducted at the ARL, sample size n=6 per ceramic composite. The test projectile includes a hardened steel core penetrator with length of 47.6 mm (1.875 in), a diameter of 10.87 mm (0.428 in) and an aspect ratio of 4, and is also known as the 12.7 mm APM2, shown in Figure 2. The nominal projectile weight was 46 grams, and core density was 7.85 g/cc.

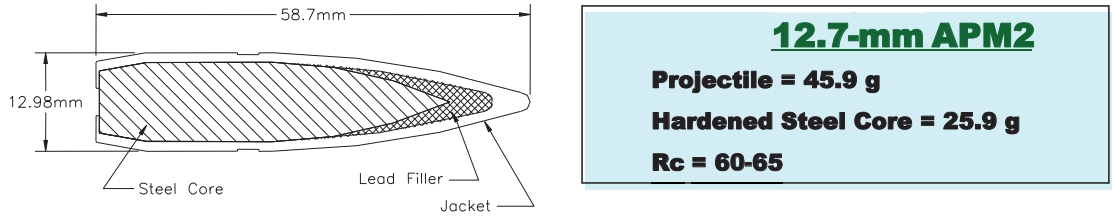

Figure 2. Cross Section of a 12.7-mm APM2.

The impact velocity used for all experiments was nominally 848 m/s (2782 ft/s), although some shots were varied from 824 m/s (2704 ft/s) up to 872 m/s (2861 ft/s) into the aluminum back plates alone to provide for DOP corrections for velocity variations. The velocity was chosen in order to produce a range of practical residual penetrations while being consistent with normal operating conditions.

Projectiles with 3 degrees or greater of total yaw were excluded from analysis; as previous studies had indicated this as an appropriate cutoff point for ballistic tests at zero obliquity. Measurement of the projectile yaw and velocity was accomplished using a Hewlett-Packard 150 kV Flash X-Ray System in 2 orthogonal planes

All residual penetration measurements were obtained by sectioning the AA6061 plates. A bandsaw was used to section all penetration cavities, and measurements were made using Vernier calipers to the deepest portion at the cavity, as indicated in Figure 3. Measurement of the "a" value avoids errors which could be caused by deformation of the aluminum block around the entrance cavity.

https://doi.org/10.52202/078352-0001

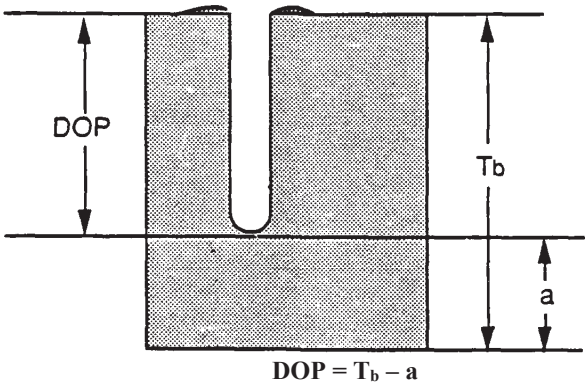

Figure 3. Measurement of Residual Penetration.

The contribution of the dynamic failure mechanisms (stiffness, deceleration) attributed to the aluminum tiles, which contributed to the performance of the aluminum plates, were normalized through deconstructing their interference employing a proprietary algorithm.

3.0 Results and Discussion

3.1 Material Characterization

Across nine plates, the density of the material was measured to be 2.370 g/mL with a standard deviation of 0.010 g/mL. This show the process results in material that is relatively homogeneous between plates, as there is little variation in density.

https://doi.org/10.52202/078352-0001

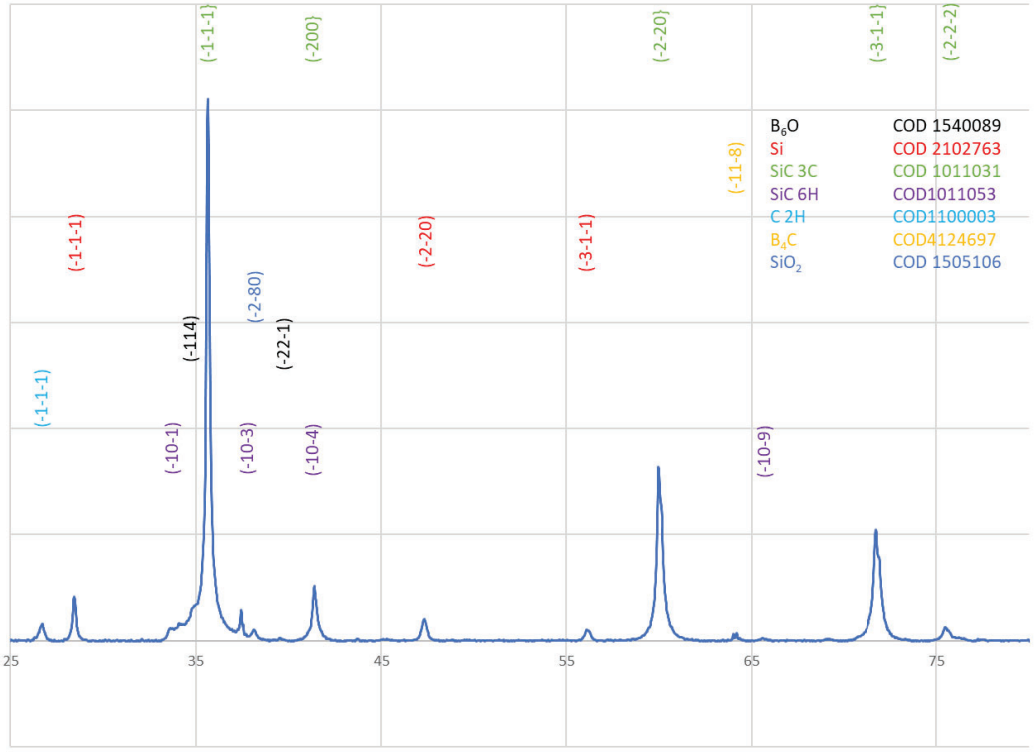

Figure 4. X-ray diffraction pattern of the sample plate with Miller indices of the identified phases for each peak listed.

The composition of the sample was determined by analyzing the X-ray diffraction pattern shown in Figure 4. Each peak is marked with Miller indices in a color corresponding the identified phase. Identification was made using the Crystallography Open Database (COD), with the pattern number used for identification listed in the legend. SiC-3C, SiC-6H, Si, B_6O, and graphite are present. The most common form of SiC in the samples is SiC-3C or β-SiC. This is the form of SiC that results from pyrolysis and crystallization of a polymer precursor. While BN was added to the constituent paste, no BN is present in the sample plate. While Si was added to react with residual carbon in the sample and aid densification, Both Si and graphite are present in the manufactured plate. These phases are generally considered detrimental to ballistic performance.

Figure 5. Optical photograph of polished cross-section that was cut parallel to the z-direction.

Figure 5 shows a cut and polished cross-section of a manufactured plate. The material in the plate was quite inhomogeneous, which was evident in the varying shades through the sample. This homogeneity seemed to correspond to the concentration of SiC whiskers. Significant cracking was visible throughout the microstructure. This would be highly detrimental to any mechanical or armor applications.

https://doi.org/10.52202/078352-0001

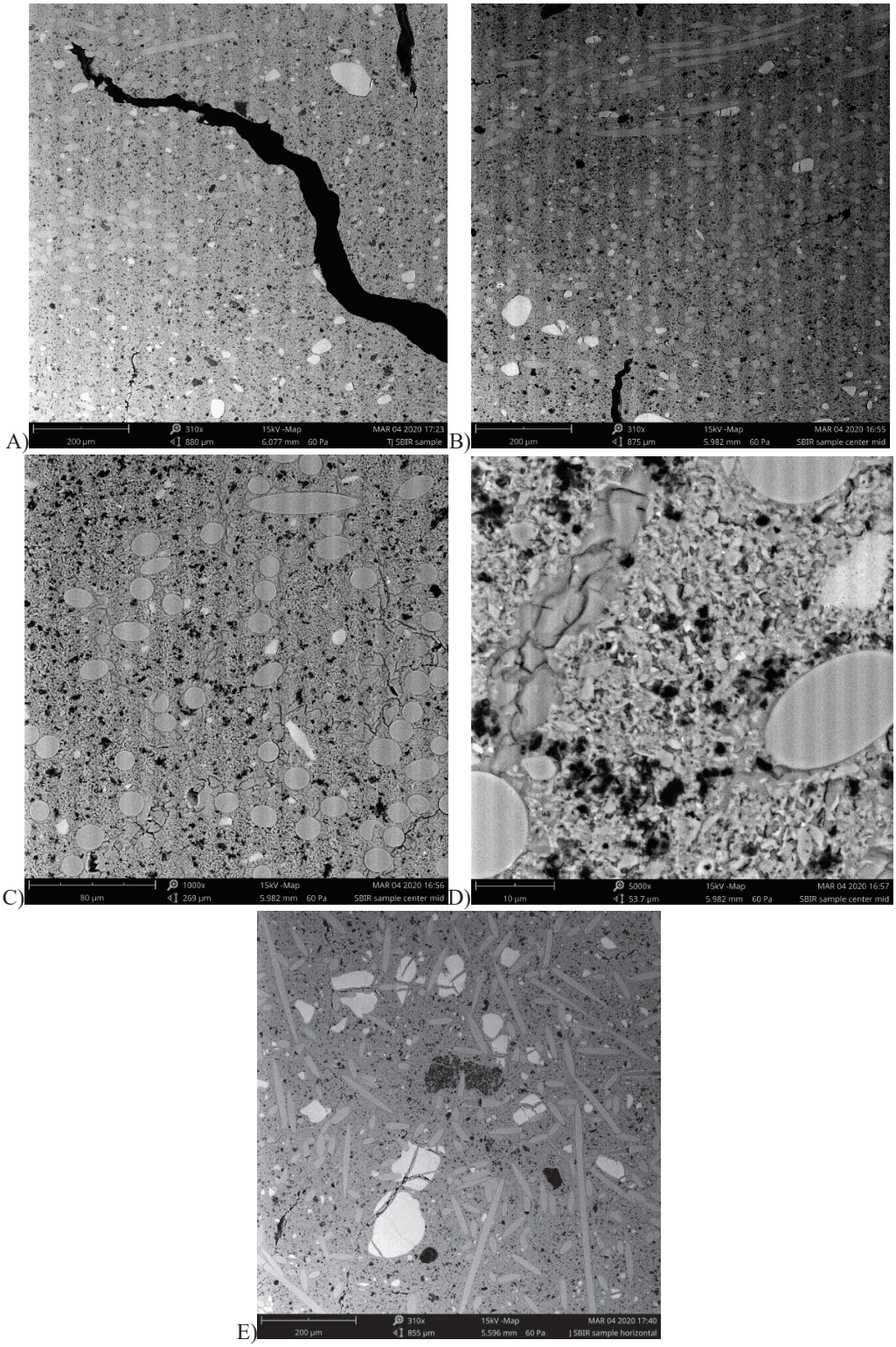

Figure 6. Microstructural images of the plate material. Image A was taken from a cross-section parallel to the z-direction. Taken from the same cross-section, Images B-D show another area of the sample at successively higher magnifications. Image E was taken from a cross-section perpendicular to the z-direction

https://doi.org/10.52202/078352-0001

Beyond optical imaging, SEM imaging was conducted to view the microstructure. Figure 6A shows the tip of a crack that was visible optically in Figure 6. The size of the crack opening makes the authors believe it is process related, likely from the polymer infiltration pyrolysis (PIP) process. Polymer derived ceramic precursors undergo significant shrinkage during conversion which can cause such fissures in the final ceramic. Figure 6B shows a separate area of the same cross-section, with many circular cross-sections of SiC whiskers of about 20 microns in diameter present. There is an increase in concentration of whiskers from area to area. Also visible are many dark black patches and large (50-60 micron) bright grains, which are identified as graphite and Si, respectively. Both materials are generally believed to be detrimental to armor performance, as they act as crack initiators. At the higher magnification shown in Figure 6C, fine cracks can be seen running around the interfaces between the SiC whiskers and fine-grained matrix material. These cracks are likely due to the coefficient of thermal expansion mismatch between the materials occurring during the heating cycles. At an even high magnification shown in Figure 6D, the individual micron-sized grains can be viewed.

Figure 6E shows a cross-section of the plate taken perpendicular to the z-direction. The cross-section of the SiC whiskers have a much higher aspect ratio when compared to the images in Figure 6A and 6B. This shows the orientation of the whiskers along this plane. Also visible in this area are large Si grains and agglomerates of graphite.

Hardness of the surface and cross section of the material were measured from a 6 x 6 grid of indents with 600 µm spacing in both X and Y directions, shown in Figure 7. The hardness of the cross sectioned material was 5.0 ± 1.57 GPa, with a large variability of 2.6 GPa to 7.6 GPa, in hardness from using 24 data points. The sample surface had a hardness of 6.4 ± 0.78 GPa with a variability from 520.5 to 8.2 GPa. The increase in hardness of the surface may be due to an increase of whiskers aligned parallel to the surface (long aspect of the whisker) leading to an increase in indent interaction with the whiskers. There was no observed excessive spall around the indents.

Data points were removed due to the indent being to asymmetric, >12%, and/or having a second phase at either the crack tips or center of the indent.

3.2 Dynamic Impact Characterization

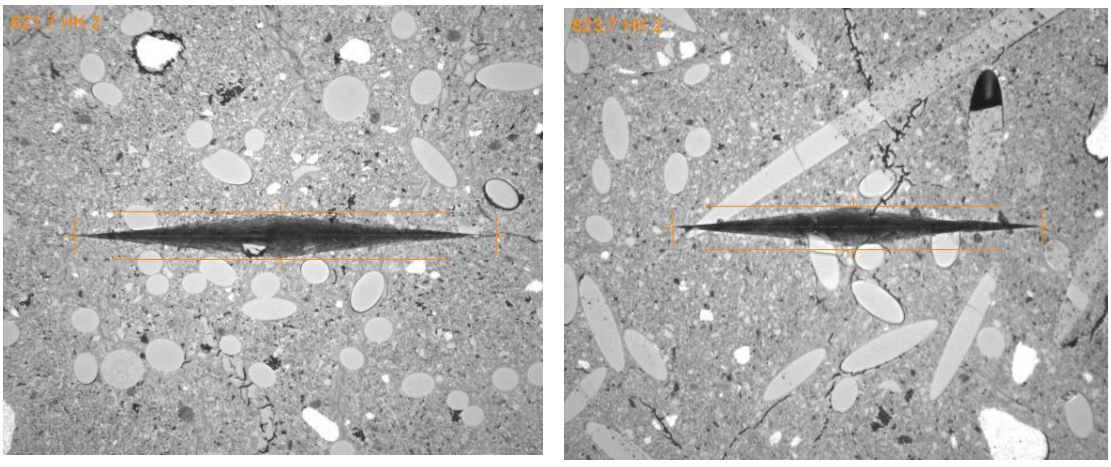

Figure 7. Optical images of 2 kgf Knoop indents on the cross section (left) and the surface (right) of the samples provided.

https://doi.org/10.52202/078352-0001

Six targets comprised of SiC tiles from Goodman Technologies were ballistically evaluated in accordance with experimental procedures reported in ARL-TR-7768 [4]. Each target was fully supported in the test rig by two C-clamps fixed on opposite sides of the target, to two vertical frames, as shown in Figure 8.

A) Front View B) Side View

Figure 8. Test setup for SiC targets in ballistic investigation.

The reference velocity for each target-penetrator interaction was 848 m/s. Post-test, the six targets were cut down the center of impact, labeled by shot number, and measured for depth of penetration, shown in Figure 9. The depth of penetration of the impacted targets ranged from 51 mm to 64 mm.

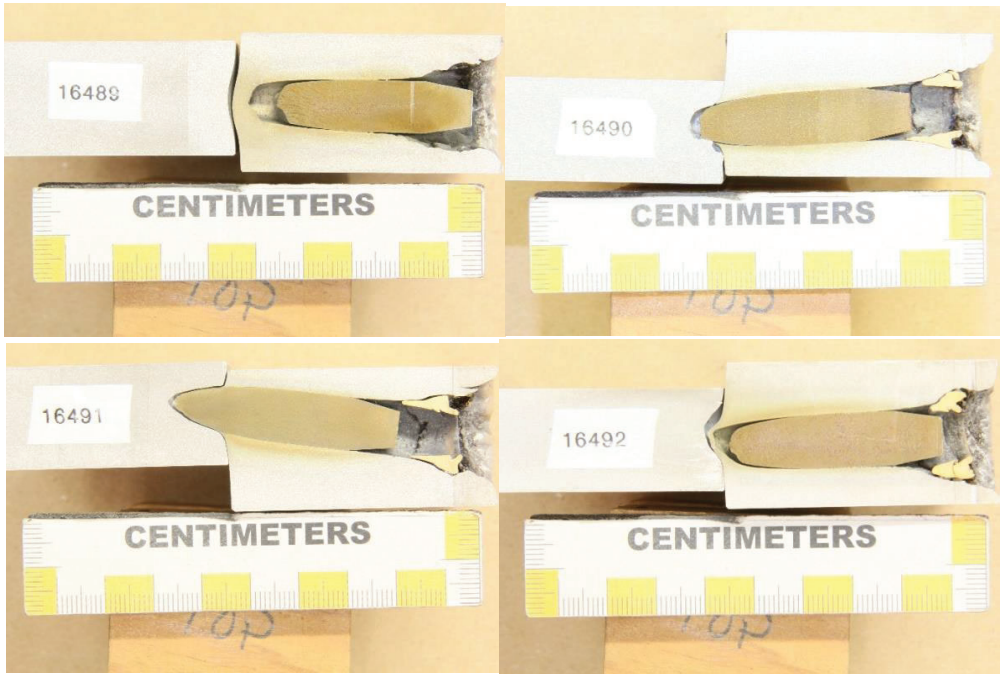

https://doi.org/10.52202/078352-0001

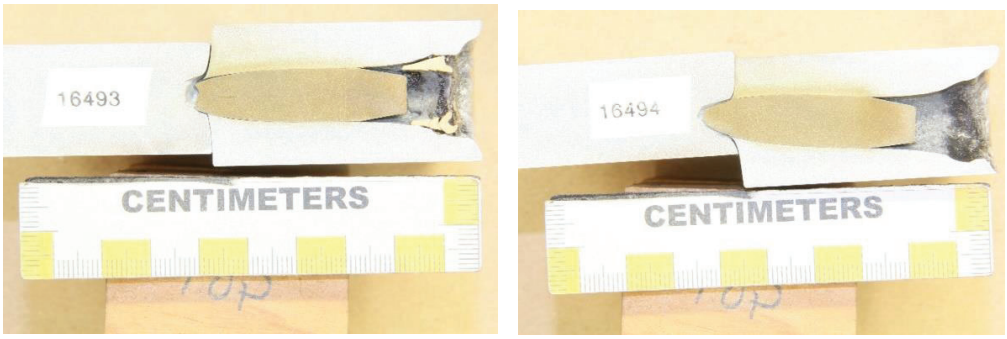

Figure 9. Cross section of 12-mm APM2 penetrator in target.

The depth of penetrations were normalized to the performance of the witness AA6061 witness plate. Finally, the ceramic efficiency, Cp, of each ceramic was calculated against the AA6061 witness plate, Figure 10. The density of versus the normalized depth of penetration into the witness plate was plotted for each SiC tile. The minima of each level of ceramic efficiency is shown as slash-dot lines. The ceramic efficiency of traditionally manufactured CoorsTek SiC, measured in an earlier experiment, is added for parametric analysis [4]. While the density of the z-processed SiC was lighter than the density of CoorsTek SiC (2.37 g/mL versus 3.21 g/mL), the ceramic efficiency of z-processed SiC was 42% of the CoorsTek SiC (6.94).

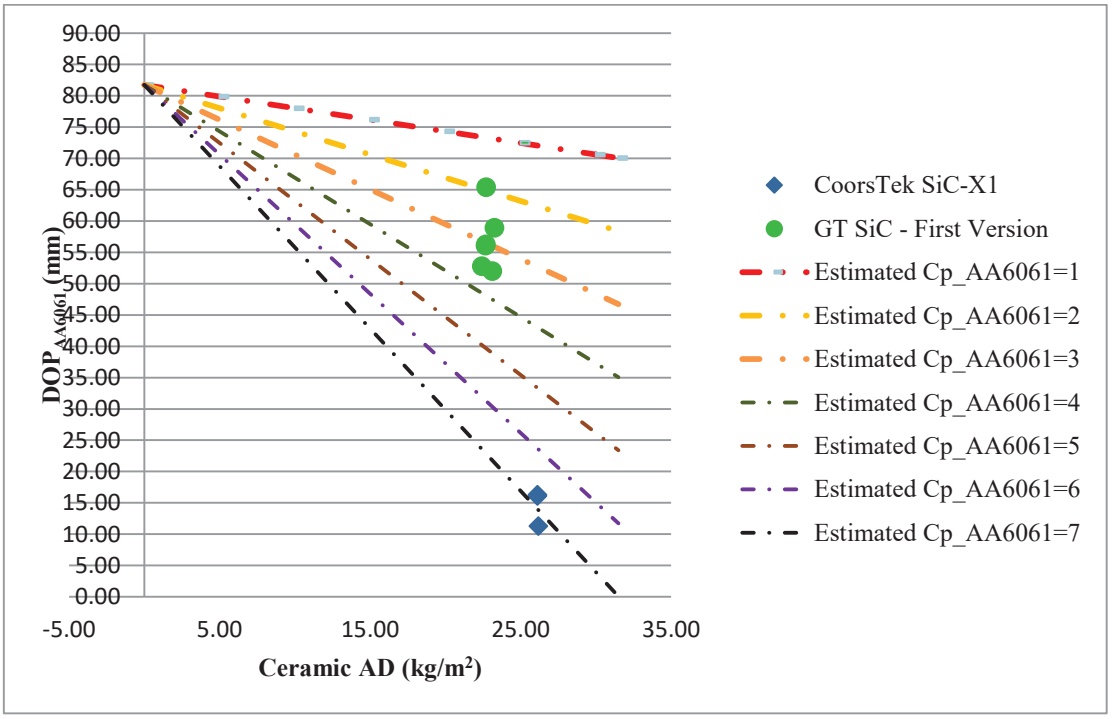

Figure 10. Ceramic efficiency of SiC tiles.

https://doi.org/10.52202/078352-0001

4.0 Conclusion

The manufactured plates consisted of a heterogeneous blend of β-SiC, α-SiC, Si, B_6O, and graphite. BN, one of the constituent material of the printed paste, was not found in the plate and may have reacted during processing. The microstructure of the material consisted of multiscale features, with large SiC whiskers and Si grains as well as fine, micron-sized SiC grains. Orientation of the whiskers was found to be align to the plane perpendicular to the z-process direction. Extensive multiscale cracking was also found through the sample. Larger fissure-like cracks are inferred to be caused by the volumetric shrinkage expected during the PIP process, with the fine crack around whisker interfaces due to thermal mismatch of the blended material. From a material perspective, the residual Si and graphite phase as well as multiscale cracking can be detrimental to ballistic performance of the plate. In ballistic studies, the 12.7 mm APM2 projectile penetrated the z-processed SiC tiles at 70% more depth than the CoorsTek SiC tiles. One primary reason for the degradation in performance is the lack of work on the nose of the projectile during the target-projectile interaction. Future research will examine the relationship between the multiscale cracks of the z-processed SiC and the effect on ceramic armor mechanisms during ballistic impact.

5.0 Acknowledgements

The authors would like to acknowledge Clifford Hubbard and William Gamble for their technical expertise and assistance. The authors would like to acknowledge the technicians Donnie Little and Perry Peregino for their ballistic assistance.

6.0 References

[1] Secretary of the Army approves new advanced manufacturing policy, U.S. Army Public Affairs, October 4, 2019, https://www.army.mil/article/228151/secretary_of_the_army_approves_new_advanced_manufacturing_policy.

[2] Enabling Readiness and Modernization Through Advanced Manufacturing, also called the Army Advanced Manufacturing Initiative (AAMI), September 18, 2019, https://armypubs.army.mil/epubs/DR_pubs/DR_a/pdf/web/ARN19451_AD2019-29_Web_Final.pdf.

[3] Encouraging Innovation in Manufacturing, A Presidential Document by the Executive Office of the President, February 26, 2004, https://www.federalregister.gov/documents/2004/02/26/04-4436/encouraging-innovation-in-manufacturing.

[4] Tyrone L Jones, Jeffrey Swab, Christopher S Meredith, and Benjamin Becker, The First Static and Dynamic Analysis of 3-D Printed Sintered Ceramics for Body Armor Applications, ARL-TR-7768, Aberdeen Proving Ground, MD, September 2016.

https://doi.org/10.52202/078352-0001